Generalized Scaling Law for Exciton Binding Energy in Two-Dimensional Materials

S. Ahmad,[1,§] M. Zubair,[2,*,§] O. Jalil,[1] M. Q. Mehmood,[2] U. Younis,[1,3,†] X. Liu,[3] K. W. Ang,[4] and L. K. Ang[5,‡]

[1] *Electrical Engineering Department, Information Technology University (ITU) of the Punjab, Lahore 54000, Pakistan*

[2] *NanoTech Lab, Electrical Engineering Department, Information Technology University (ITU) of the Punjab, Lahore 54000, Pakistan*

[3] *College of Materials Science and Engineering, Shenzhen Key Laboratory of Microscale Optical Information Technology, Chinese Engineering and Research Institute of Microelectronics, Shenzhen University, 3688 Nanhai Avenue, Shenzhen 518060, People's Republic of China*

[4] *Department of Electrical and Computer Engineering, National University of Singapore, 4 Engineering Drive 3, Singapore 117583, Singapore*

[5] *Science and Math Cluster, Singapore University of Technology and Design (SUTD), 8 Somapah Road, Singapore 487372, Singapore*

(Received 30 January 2020; revised manuscript received 30 March 2020; accepted 22 May 2020; published 25 June 2020)

Binding energy calculation in two-dimensional (2D) materials is crucial in determining their electronic and optical properties pertaining to enhanced Coulomb interactions between charge carriers due to quantum confinement and reduced dielectric screening. Based on full solutions of the Schrödinger equation in a screened hydrogen model with a modified Coulomb potential $(1/r^{\beta-2})$, we present a generalized and analytical scaling law for the exciton binding energy, $E_\beta = E_0(a\beta^b + c)(\mu/\epsilon^2)$, where β is a fractional-dimension parameter that accounts for the reduced dielectric screening. The model is able to provide accurate binding energies, benchmarked using the reported Bethe-Salpeter equation and experimental data, for 58 monolayer 2D and eight bulk materials, respectively, through β. For a given material, β is varied from $\beta = 3$ for bulk three-dimensional materials to a value lying in the range 2.55–2.7 for 2D monolayer materials. With $\beta_{\text{mean}} = 2.625$, our model improves the average relative mean square error by a factor of 3 in comparison to existing models. The results can be used for Coulomb engineering of exciton binding energies in the optimal design of 2D materials.

DOI: 10.1103/PhysRevApplied.13.064062

I. INTRODUCTION

Accurate determination of optical and electronic properties of bulk and two-dimensional (2D) materials is crucial for many applications, especially when the excitonic effects become significant in the 2D regime due to structural changes induced by dielectric environments leading to variation in binding energies [1–10]. The 2D nature of the material makes the excitons easily tunable, with some external stimuli, enabling excitonic-transport-based photonic devices such as electrically driven light emitters, optovalleytronic devices, photovoltaic solar cells, and lasers [11–13]. Thus the binding-energy calculation in 2D materials has become an active area of research and numerous studies based on theoretical and experimental approaches have been reported in the literature to understand the excitonic effects and their implications [14–18]. Due to the high cost of experimental procedures, reliance on numerical approaches such as the Bethe-Salpeter equation (BSE) becomes inevitable for accurate modeling of excitonic effects and thus serves as a benchmark for other models [19]. In order to reduce the computational complexity, analytical methods are desirable to speed up the design processes [20–22]. A number of models to describe exciton behavior have been reported, including the pioneering works of Frenkel and Wannier-Mott (W-M) [23,24]. The Frenkel model is based on the concept of localized screening, whereas the W-M model incorporates an average delocalized screening effect irrespective of the actual dielectric environment and thus leads to an overestimation of binding energies. Olsen *et al.* [25] introduced an effective dielectric screening based on material polarizability, resulting in relatively accurate binding

*muhammad.zubair@itu.edu.pk
†usman.younis@itu.edu.pk
‡ricky_ang@sutd.edu.sg
§These authors contributed equally to this work.

energies. Recently, a generalized extension of the model by Jiang *et al.* [26] has found the 2D exciton binding energy to be one fourth of the band gap, resulting in error reduction. The difficulty with the existing models is that the inherent Coulomb screening potential does not take the structural-confinement effects into account and therefore the accuracy in 2D binding-energy calculations is compromised. Therefore, we propose a simple approach to explicitly incorporate the structural-confinement effects in the screening potential by representing the Coulomb potential in a fractional space to represent a more realistic dielectric environment in an effective manner. Moreover, the realistic systems are not 2D in a strict sense and the fields, including the electric field and the magnetic field, the electron emission, and the angular momentum, are not confined to a smooth plane [27]. Hence, the central force between the electron and the nucleus may be better represented by a generalized Coulomb potential function, assuming that the system lies in an equivalent fractional-dimensional space. It is worthwhile to mention that the concept of fractional-dimensional space has been successfully applied to study the effects of confinement, roughness, and disorder in various physical problems arising in electron-device modeling [28,29], plasma physics [30], and electromagnetism [31].

Motivated by the above, the purpose of this paper is fourfold.

First, an analytical model based on the power-law fit to the full solution of the simple hydrogen model with a fractional Coulomb potential is presented, of the form $E_\beta = E_0(a\beta^b + c)(\mu/\epsilon^2)$, namely the fractional Coulomb potential (FCP) model, where β is a fractional-dimension parameter linked to the screened Coulomb potential, $E_0 = 13.606$ eV is the Rydberg energy, $a = -2.619 \times 10^4$, $b = -9.634$, $c = -0.3833$, and μ and ϵ represent the material-specific reduced exciton effective mass and dielectric constant, respectively.

Second, we demonstrate the accuracy of the proposed FCP model to calculate the 2D and bulk binding energies, benchmarked using the BSE and experimentally reported data. The FCP model allows the incorporation of the structural-confinement effects and enables the calculation of exact 2D binding energies corresponding to the actual dielectric environments through the fractional-dimension parameter β, with bulk values intercepted at $\beta = 3$ and monolayer data represented by β lying in the range 2.55–2.7. We also show that the W-M model is a special case of the FCP model reduced at a fixed $\beta = 2.515$.

Third, we report a correction in the average 2D exciton screening represented at $\beta_{\text{mean}} = 2.625$, based on error analysis of our proposed FCP model in comparison with existing models by using BSE-reported data for 58 monolayer materials having binding energies up to 1.5 eV as a reference. It is shown that binding-energy calculations based on W-M and Jiang *et al.* [26] have average mean square errors (MSEs) of 39.2% and 26%, respectively, whereas the proposed FCP model (at $\beta_{\text{mean}} = 2.625$) reduces the average MSE to below 12.8%.

Finally, we show that there exists a simple scaling with a smooth transition of β corresponding to structural confinement from bulk to the monolayer regime.

II. FORMULATION

The FCP model is based on a fractional Coulomb potential embedded in an infinite quantum well given by the radial part of a simple hydrogen model as

$$\left[-\frac{\hbar^2}{2\mu}\frac{d^2}{dr^2} + V_{\text{frac}}(r)\right]\psi(r) = E\psi(r), \tag{1}$$

where $\mu = 0.9995m_0$ ($m_0 = 9.11 \times 10^{-31}$ kg) is the exciton reduced mass, r is the radial distance, and $V_{\text{frac}}(r)$ is the fractional Coulomb potential. The fractional Coulomb potential is a generalized form of the standard Coulomb potential that exhibits a Coulomb-like electron-hole pair interaction and is based on the fractional-dimensional Poisson equation [31–33] of the form

$$\nabla_\beta^2 V_{\text{frac}}(r) = -\rho/\epsilon, \tag{2}$$

where β is a fractional-dimension parameter that is valid in the range $2 < \beta \leq 3$, ρ is the volume charge density, and ∇_β^2 is a generalized fractional-dimensional Laplacian operator in spherical coordinates [34], with the radial component given by

$$\nabla_\beta^2 = \frac{1}{r^{\beta-1}}\frac{\partial}{\partial r}\left[r^{\beta-1}\frac{\partial}{\partial r}\right]. \tag{3}$$

Following the analytical solution of Eq. (2) from Ref. [32], the fractional Coulomb potential takes the form

$$V_{\text{frac}}(r) = k_\beta e^2/r^{\beta-2}, \tag{4}$$

where $k_\beta = \Gamma(\beta/2)/[2\pi^{\beta/2}(\beta-2)\epsilon_0]$. At $\beta = 3, k_\beta$ reduces to $1/4\pi\epsilon_0$ and $V_{\text{frac}}(r)$ simplifies to the standard Coulomb potential of the form $1/r$. When β differs from three, the Coulomb potential of a point source falls off as $1/r^{\beta-2}$ and the dynamical symmetry is broken; this is effectively linked to the reduced hydrogenic screening and leads to an effective reduction in the Bohr radius.

The full solution to Eq. (1) is performed (for the detailed derivation, see the Appendix) to calculate the ground-state hydrogenic energy $e_0(\beta)$, where $e_0(\beta) = E_0(\beta)/13.6$ eV. A power-law fit to the full solution of Eq. (1) is performed to develop an analytical scaling law for the binding-energy

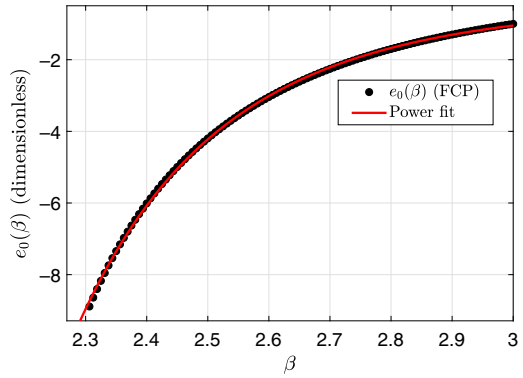

FIG. 1. Curve fitting to FCP computed ground-state hydrogenic energies for $2 < \beta \leq 3$, based on full solution. The markers indicate the FCP data points. The dotted line presents the power-law fit to the data with the function $e_0(\beta) = a\beta^b + c$, where $a = -2.619 \times 10^4$, $b = -9.634$, and $c = -0.3833$, with 95% confidence bounds of $(-2.867 \times 10^4, -2.37 \times 10^4)$, $(-9.749, -9.519)$, and $(-0.4164, -0.3502)$, respectively.

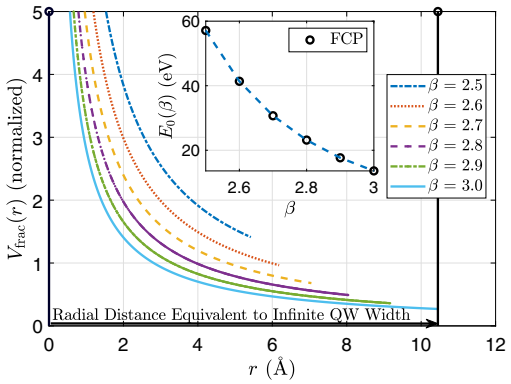

FIG. 2. An illustration of the FCP model with an analogous example of an infinite QW model. The radial distance corresponds to the QW width, taken as being at least 20 times the Bohr radius, in order to converge the full solution of the FCP model in Eq. (1) for ground-state hydrogenic energies, as shown in the inset. The FCP model reduces to a standard hydrogen model at $\beta = 3$ with $E_0(\beta) = 13.6$ eV, whereas for $2 < \beta < 3$, the FCP model reflects a screened hydrogen model and thus results in $E_0(\beta) > 13.6$ eV. The screened hydrogen model corresponds to an infinite QW model, having the provision to vary the QW width through β.

calculation, given by

$$E_\beta = E_0\left(a\beta^b + c\right)\left(\frac{\mu}{\epsilon^2}\right), \tag{5}$$

where $E_0 = 13.6$ eV, $a\beta^b + c \approx e_0(\beta)$, $a = -2.619 \times 10^4$, and $b = -9.634$ and $c = -0.3833$ are the fitting parameters obtained from a power-law fit to $e_0(\beta)$ with 95% confidence intervals of $(-2.867 \times 10^4, -2.37 \times 10^4)$, $(-9.749, -9.519)$, and $(-0.4164, -0.3502)$, respectively, as shown in Fig. 1. Here, ϵ is the dielectric constant, calculated using $\frac{1}{2}(1 + \sqrt{1 + 32\pi\alpha\mu/3})$, which represents the effective linear screening for the strict 2D case [25], μ is the reduced exciton mass, and α is the 2D polarizability based on reported data for G_0W_0 [19].

An infinite quantum-well (QW) equivalence of the FCP model in Eq. (1) is demonstrated to explain an effective reduction in the Bohr radius. The fractional Coulomb potential for $2.5 \leq \beta \leq 3$ is calculated using Eq. (4) and is plotted against a radial distance r corresponding to $\beta = 3$, as illustrated in Fig. 2. A radial distance of approximately 20 times the Bohr radius ($19.75a_0$, where $a_0 = 0.529$ Å) with a uniform mesh grid of 300 points is taken to emulate the full-wave behavior of the FCP model, which is necessary for convergence (for details, see the Appendix). Here, the radial distance is equivalent to an infinite QW width and is highlighted to shrink with decreasing values of β. This is validated by first computing the ground-state hydrogenic energies $E_0(\beta)$ for $2.5 \leq \beta \leq 3$ using the FCP model in Eq. (1), as shown in the inset of Fig. 2. The resulting values of $E_0(\beta)$ are then employed to calculate the corresponding infinite QW width w, using

$$w = \sqrt{\hbar^2\pi^2/2\mu E_0(\beta)}, \tag{6}$$

which is in excellent agreement with the radial distance r as shown in Fig. 3. The decrease in w corresponds to a reduction in the effective Bohr radius given by $a_\beta = w/19.75$, as illustrated in the inset of Fig. 3. The reduction in a_β takes place due to a proportionate decrease in the QW dimensions, as a well width of at least $19.75a_\beta$ is required for the infinite QW model to produce hydrogenic energies $E_0(\beta)$.

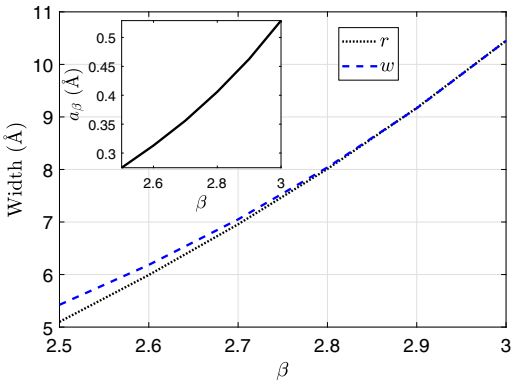

FIG. 3. A demonstration of the FCP model as an equivalent infinite QW model. The black dotted line shows the corresponding decrease in the radial distance with β, as depicted in Fig. 2. The blue dashed line is the equivalent reduction in the infinite QW width calculated using Eq. (6), corresponding to ground-state hydrogenic energies calculated using the FCP model in Eq. (1) for $2.5 \leq \beta \leq 3$. The inset shows a reduction in the effective Bohr radius calculated as $a_\beta = w/19.75$, where w is the infinite QW width for $2 < \beta \leq 3$.

III. RESULTS AND DISCUSSION

The significance of the fractional Coulomb potential in the 2D binding-energy calculation is highlighted by performing a comparison of the existing analytical methods with the proposed FCP model by using BSE-reported binding energies for 58 monolayers as a benchmark [19]. The analysis is performed to intercept β based on the FCP model in Eq. (5) for binding energies reported using the BSE and that calculated using existing analytical models. The result in Fig. 4 shows that the FCP model accurately produces results through β, with most of the monolayer materials found to lie at β values in the range 2.55–2.7, to represent the actual 2D exciton screening, whereas the W-M model is shown to overestimate the 2D binding energies, with the average screening represented by a fixed value of $\beta = 2.515$ as a special case. This is because the W-M model considers the average screening in 2D excitons with binding energies given by $4 \times (13.6\mu/\epsilon^2)$ [27]. However, the exciton model given by Jiang *et al.* [26] results in significant under- or overestimation of binding energies. Moreover, the FCP model is also demonstrated to intercept binding energies for eight bulk materials at $\beta = 3$, benchmarked using experimentally reported data [35–46].

The fractional-dimension parameter β is linked to the screening effect due to the fractional Coulomb potential. It is related to the dimensionality in terms of the hydrogenic Bohr radius, explained through the equivalence of the proposed FCP model to an infinite QW model and, in fact, is not directly related to the physical dimensions. It has been shown in Fig. 4 that $\beta = 3$ and $2.55 \leq \beta \leq 2.7$ represent the bulk and 2D screening, respectively. The Coulomb potential in fractional space provides an additional parameter in the form of β, in addition to μ and ϵ, which allows us to incorporate a screening correction in material systems induced due to the varying thickness, substrates, and stress layers and the practical conditions under which the experimental and numerical calculations are performed.

The result in Fig. 5 illustrates an error analysis of the proposed FCP model in comparison with existing models by using BSE-reported data for 58 monolayer materials as a reference. The BSE data are calculated accurately by the FCP model fitted with the respective β values, whereas the W-M data, having an inherently fixed $\beta = 2.515$, show an overestimation that increases with the binding energies. However, the exciton model by Jiang *et al.* [26] has a variable β and is shown to exhibit an increase in underestimation for binding energies greater than 0.5 eV. Moreover, the existing models capture reported values in good agreement limited up to 0.5 eV, as also reported by Olsen *et al.* [25]. This limitation is caused by the incorrect dielectric screening in the existing models, which is validated by the FCP model, with the identification of actual average screening represented at $\beta_{\text{mean}} = 2.625$. This corrected β is found to result in binding energies that fall comparatively, in good agreement with the reported BSE data up to 1.5 eV. The result in Fig. 6 shows an average reduction in the relative MSE for the FCP model with $\beta_{\text{mean}} = 2.625$ to less than 12.8%, which is a reduction of approximately one third and one half in comparison to W-M and Jiang *et al.* [26], respectively.

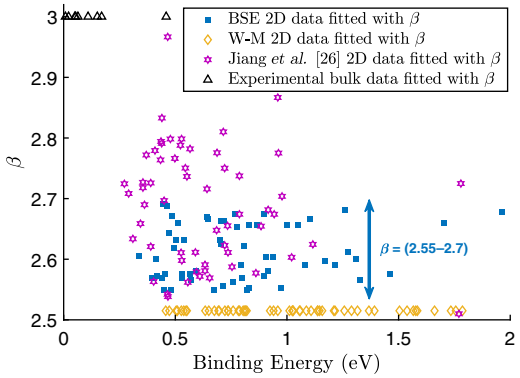

FIG. 4. The FCP model in calculations based on Eq. (5), to intercept β for 58 monolayer materials for reported values of BSE binding energies [19], W-M data calculated for 58 monolayer materials using $4 \times (13.6\mu/\epsilon^2)$ and fitted with the respective β values [24,47], Jiang *et al.* [26] data calculated for 58 monolayer materials with $E_g/4$ and fitted with the respective β values, and experimentally reported data for eight bulk materials also fitted with the respective β values. Here, it is to be noted that the binding-energy calculation for the aforementioned models is performed by employing the required reported data: the complete details are given in the Supplemental Material [48]. The blue double-headed arrow shows the range of β for 2D BSE data.

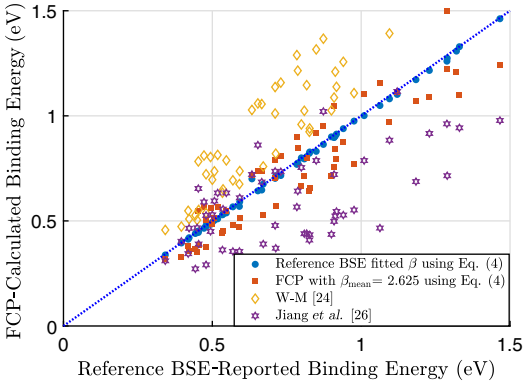

FIG. 5. A comparative analysis of the relative MSE in calculated binding energies for the FCP model with $\beta_{\text{mean}} = 2.625$ using Eq. (5), W-M, and Jiang *et al.* [26] with respect to reported BSE data fitted with the respective β values, using Eq. (5) taken as a reference. Binding energies calculated using the FCP model with $\beta_{\text{mean}} = 2.625$, capable of capturing most of the data in comparatively good agreement up to 1.5 eV, in contrast to 0.5 eV for the other two models.

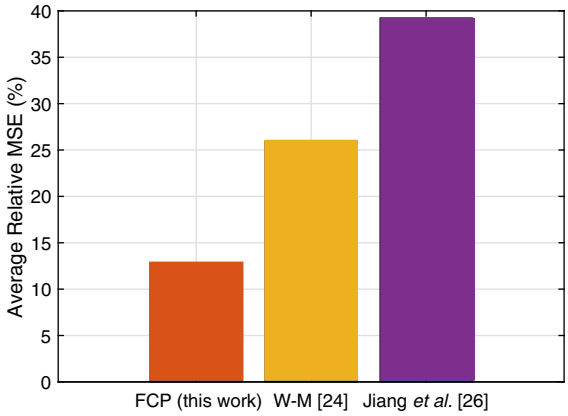

FIG. 6. The FCP calculation with $\beta_{\text{mean}} = 2.625$ reduces the relative average MSE for 58 monolayer materials up to one half and to one third in comparison to Jiang *et al.* [26] and W-M, respectively. Moreover, a comparison with Olsen *et al.* [25] shows an approximate reduction in the error of up to one fourth (for details, see the Supplemental Material [48]).

It is to be noted that the simple screened hydrogen model with the classical Coulomb potential with a $1/r$ dependence demonstrates W-M excitons of a delocalized nature and hence can model binding energies of a few hundreds of millielectronvolts correctly. Since the dielectric screening in some 2D materials can be greatly reduced, the exciton binding energy may reach higher values (up to 1 eV and above). However, their corresponding quasiclassical radius of the ground-state orbital may still remain substantially larger than the lattice constant [49]; such excitons can be regarded as W-M excitons and are sometimes referred to as tightly bound 2D W-M excitons. Here, the materials with higher binding energies are presumed to fall into this category of tightly bound 2D W-M excitons and our FCP model with its $1/r^{\beta-2}$ dependence can model them correctly. Once the exciton radius becomes comparable to the lattice constant, the strongly W-M picture becomes inapplicable and a non-Coulombic electron-hole interaction takes place [49,50], which is beyond the scope of the current study. Moreover, binding energies smaller than 0.35 eV are not subject to experiment due to limited availability of the reference data; the materials included in this work have a high dynamic and thermodynamic stability with the available reference values of the BSE binding energy, the G_0W_0 band gap, the effective mass, and the 2D polarizability [19].

The FCP model intercepts the BSE-reported 2D binding energies based on a hydrogenic solution with the Coulomb potential represented in the fractional space by including an effective linear screening based on 2D polarizability and additionally allows for the correction in 2D screening through β, resulting in a Bohr radius corresponding to a 2D regime. Further, an exciton radius of 5.53 Å is calculated for monolayer MoS_2 as $R_{\text{exc}} = a_\beta(\epsilon/\mu)$, corresponding to a binding energy of 0.547 eV, intercepted at $\beta = 2.631$. Here, $\mu = 0.236$, $\epsilon = 4.003$, and $a_\beta = 0.326$ Å is calculated as $w/19.75$, where w is equal to 6.44 Å computed at $\beta = 2.631$, using the result in Fig. 3. The calculated value of 5.53 Å is in good agreement with the theoretically reported value of approximately 5.5 Å [51] corresponding to an experimentally reported monolayer thickness of approximately 0.65 nm [52]. Although an exciton radius of 1 nm has also been reported [21,53], corresponding to varying values of binding energies for free-standing monolayers of 0.96 eV and 0.54 eV, the authors do not explain why the exciton radius does not change: a change in the radius is linked to the screening [54] and the screening effect has been shown to change the binding energies [55]. We believe that such discrepancies can arise due to different approaches chosen to initiate the numerical calculations and that a further investigation in the future will prove to be fruitful.

A smooth transition of β with structural confinement from bulk to the monolayer, given the material data for the respective number of layers, is presented in Fig. 7. This demonstration is based on a power-law fit to the reported MoS_2 binding energies corresponding to a decreasing number of layers, intercepted with the FCP model through β as given in Table I. In practice, the variation of the binding energy is inversely proportional to the dielectric constant, whereas the dielectric constant is known to have a direct relationship with the structural confinement [56,57], due to which the proposed FCP model can provide an approximate estimate of the layer thickness corresponding to the desired binding energy through the mapping of the fractional-dimension parameter β, as demonstrated in Fig. 8. The result in Fig. 8 is an extension of Fig. 7, which shows a relationship between the fractional-dimension parameter β and the number of layers (L), given by $\beta(L)$. Here, $\beta(L)$ follows a power-law model of the form

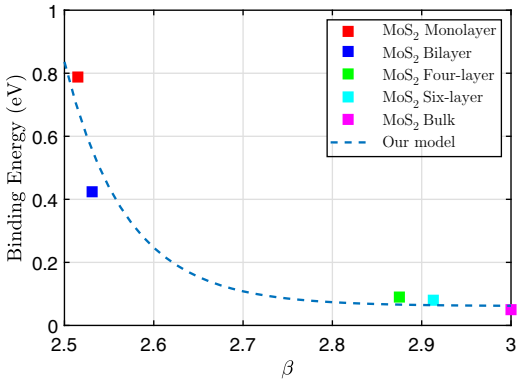

FIG. 7. A demonstration of the smooth transition of β with respect to the binding energy for MoS_2, given μ and ϵ data for the respective numbers of layers. The blue dotted line represents a power-law fit to the data points given in Table I.

TABLE I. The calculation details for FCP-model-based interception of the reported MoS_2 binding energies corresponding to a structural confinement from bulk to the monolayer.

Structure	μ	ϵ	Binding energy (eV)	Number of layers (L)	β_{FCP}[a]
Bulk	0.4 [35]	10.71 [35]	0.04 [35]	31[b]	3
Six-layer	0.3 [59]	7.92 [59]	0.08 [59]	6 [59]	2.913
Four-layer	0.25 [59]	7.16 [59]	0.09 [59]	4 [59]	2.875
Bi-Layer	0.25 [59]	5.51 [59]	0.424 [59]	2[59]	2.531
Monolayer	0.19 [47]	3.43 [47]	0.897 [47]	1 [47]	2.506

[a]The FCP-model interception of binding energies for the respective layers through tuning of β.
[b]Bulk thickness (approximately 20 nm)/monolayer thickness (0.65 nm) [52].

$(c_1 L^{c_2} + c_3)$ and indicates a sharp decrease in the screening for the 2D regime (very small L) compared to the bulk regime (large L), attributed to the strong excitonic effects due to structural confinement. This allows an approximate calculation of the binding energies for a changing number of layers as $E_{\beta,L} = E_0\big[\, a\beta(L)^b + c\big]\,(\mu/\epsilon^2)$, where a, b, and c remain the same as in Eq. (5), highlighting the usefulness of the FCP model in practical design problems. It is worthwhile to mention that an earlier model reported by Thilagam has reported the kinetic energy part of the two-particle fractional-dimensional Schrodinger equation with a classical Coulomb potential [58]. On the contrary, our FCP model demonstrates that the fractional Coulomb potential corresponds to structural changes from bulk to the 2D regime and thus provides a better representation of dielectric screening in confined materials.

As an example for many applications, recent studies on a number of photovoltaic systems based on 2D materials [60–63] have been demonstrated to highlight the influence of various dielectric environments and structural

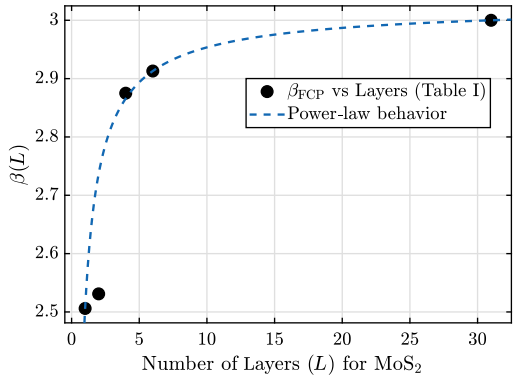

FIG. 8. A demonstration of the smooth transition of β with respect to the number of layers in MoS_2, showing the usefulness of the FCP model in the design process for practical applications. The blue dotted line shows that $\beta(L)$ follows a power-law model as $(c_1 L^{c_2} + c_3)$, which is obtained by performing a fit to the data points given in Table I, where $c_1 = -0.5233$, $c_2 = -0.8394$, and $c_3 = 3.029$ with confidence bounds of $(-1.19, 0.1439)$, $(-3.385, 1.707)$, and $(2.413,\ 3.646)$, respectively. The black markers indicate the FCP data.

configurations on the critical role of the binding energy in solar applications for a favorable dissociation of photogenerated excitons into free carriers at room temperature. Further, the 2D binding energy is reported to make a significant contribution to band-gap renormalization and is shown to vary due to the screening induced by the external dielectric environment, leading to shifts in the optical spectrum [64–66]. Thus 2D-material-based optical detection, which requires a strict optical frequency and a narrow line width, would demand an accurate determination of the binding energy. Here, the FCP model will prove to be a promising tool due to its ability to produce accurate binding energies for a wide range of 2D materials with the average screening felt by 2D excitons corrected to represent a more realistic dielectric environment, hence contributing toward the accurate determination of optoelectronic properties. Additionally, it has the potential to track the variation in binding energy due to a change in material thickness from a monolayer to many layers and thus can allow for binding-energy tunability to achieve efficient photoconversion as reported in the literature [67,68].

Furthermore, strain in 2D materials is shown to induce band-gap shifts with excitonic effects [5,69,70] and various experimental and numerical studies [71–73] have been reported recently to account for strained excitonic effects. In future, our proposed FCP model can be extended to calculate the strained binding energies by establishing a physical relationship between β and the lattice parameters corresponding to the strain levels. Such an extension can potentially be used as a tool to control the optical properties of strained 2D materials [17].

IV. CONCLUSION

In conclusion, the proposed model gives a generalized analytical expression to calculate the binding energies for a wide range of materials ranging from bulk to the 2D regime using the reported material parameters μ and ϵ. The fractional-dimension parameter $\beta = 3$ and $2.55 \leq \beta \leq 2.7$ corresponds to the actual dielectric screening in bulk and 2D materials, respectively, and thus results in an accurate calculation of the binding energies for 58 monolayer and eight bulk materials benchmarked using reported data. An

average screening in 2D excitons represented by $\beta_{\text{mean}} = 2.625$ comparatively reduces the relative MSE, on average, by up to one third with most of the materials captured by our model up to 1.5 eV, in contrast to 0.5 eV in existing models. Finally, for a given material, we show that there exists a scaling law between β and structural confinement from bulk to the monolayer, which assists in the tuning of the binding energy by varying the material thickness. The proposed FCP model will prove useful in the design and engineering of optoelectronic devices based on 2D heterostructures, due to the critical role of the binding energy in the efficient photoconversion operation. The FCP model can provide a useful tool with its analytical approach through providing accurate binding-energy estimates for 2D materials under the impact of practical dielectric environments, thus contributing toward the optimal design of optoelectronic devices.

ACKNOWLEDGMENTS

S. Ahmad and M. Zubair contributed equally to this work. S.A. is supported by the Information Technology University (ITU) doctoral fellowship. M.Z. is supported by the ITU start-up grant. M.Z. acknowledges the travel support for a summer visit under the Singapore MOE T2 grant (Grant No. 2018-T2-1-007). L.K.A. would like to acknowledge the support of the Office of Naval Research Global grant (Grant No. N62909-19-1-2047). M.Z. is grateful to Yee Sin Ang for enlightening conversations.

APPENDIX: DETAILED DERIVATION AND FULL SOLUTION OF SCREENED HYDROGEN MODEL WITH FRACTIONAL COULOMB POTENTIAL (FCP)

The FCP model is developed based on an arbitrary potential embedded in the infinite quantum well, as illustrated in Fig. 9, following the eigenvalue calculation method reported in Ref. [74].

The radial part of the simple hydrogen model in spherical coordinates incorporating the fractional Coulomb potential represents the FCP model as follows:

$$\left[-\frac{\hbar^2}{2\mu}\frac{d^2}{dr^2} + V_{\text{frac}}(r)\right]\psi(r) = E\psi(r), \tag{A1}$$

where $\mu = 0.9995m_0$ is the exciton reduced mass, $V_{\text{frac}}(r) = k_\beta e^2/r^{\beta-2}$ is the fractional Coulomb potential, r is the radial distance equivalent to the infinite QW width, and β is the fractional-dimension parameter linked to the screened Coulomb potential.

The formulation of the eigenvalue problem for a fractional Coulomb potential embedded in an infinite QW is given as $\sum_{m=1}^{n_{\max}} H_{nm}c_m = Ec_n$ and the Hamiltonian-matrix

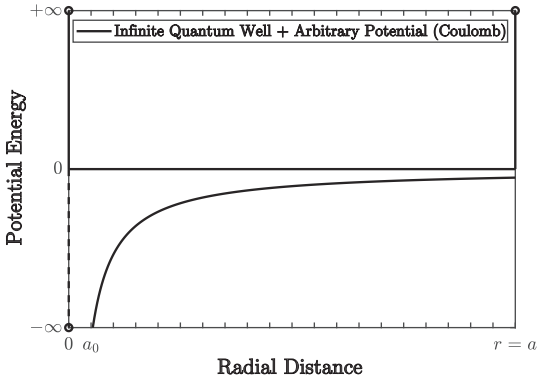

FIG. 9. The model framework for hydrogenic energy computation with the Coulomb potential embedded in an infinite quantum well. Here, a_0 is the Bohr radius and a is the radial distance of the infinite QW taken as being at least 20 times a_0 to achieve convergence. Here, we replace the Coulomb potential with a fractional Coulomb potential.

elements are given by

$$H_{nm} = \left[\langle\phi_n|H_0 + V_{\text{frac}}|\phi_n\rangle\right] = \delta_{nm}E_n^0 + V_{\text{frac}}(r), \tag{A2}$$

where $H_0|\phi_n\rangle = E_n^0|\phi_n\rangle$ represents the infinite QW. The eigenstates of the infinite QW, $\phi_n(r) = \sqrt{2/a}\sin(n\pi r/a)$, with eigenvalues $E_n^0 = \pi^2\hbar^2n^2/2m_0a^2$, allow for the Fourier-series expansion of the embedded wave function as $|\psi\rangle = \sum_{m=1}^{n_{\max}} c_m|\phi_m$, where $\int_0^\infty |\psi(r)|^2dr = 1$. The infinite QW enforces the embedding wave function $\psi(r)$ to satisfy the von Kármán boundary conditions as $\psi(0) = 0$ and $\psi(r = a) = 0$. Here, $m_0 = 9.11 \times 10^{-31}$ kg and $a = 20a_0$ is the width of the infinite quantum well. The fractional Coulomb potential over the radial distance is expressed as

$$V_{\text{frac}}(r) = -\frac{2k_\beta e^2}{a}\int_0^a \sin\left(\frac{n\pi r}{a}\right)\frac{1}{r^{\beta-2}}\sin\left(\frac{m\pi r}{a}\right)dr, \tag{A3}$$

where $k_\beta = \Gamma(\beta/2)/(2\pi^{\beta/2}(\beta-2)\epsilon_0)$. After trigonometric transformations, we arrive at

$$V_{\text{frac}}(r) = -\frac{k_\beta e^2}{a}\left[G(n+m) - G(n-m)\right], \tag{A4}$$

where

$$\begin{aligned} G(n+m) &= \int_0^a \left[\frac{1-\cos\left(\frac{\pi r}{a}(n+m)\right)}{r^{\beta-2}}\right]dr, \\ G(n-m) &= \int_0^a \left[\frac{1-\cos\left(\frac{\pi r}{a}(n-m)\right)}{r^{\beta-2}}\right]dr. \end{aligned} \tag{A5}$$

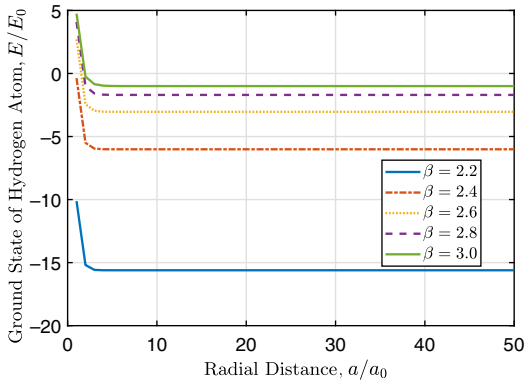

FIG. 10. The FCP-model convergence calculated by varying the radial distance a/a_0 for $n_{\max} = 400$, $E_0 = 13.6$ eV, and $a_0 = 0.529$ Å.

The dimensionless version of the Hamiltonian matrix equation for the FCP model is represented as

$$\sum_{m=1}^{n_{\max}} h_{nm} c_m = e c_n, \tag{A6}$$

where $h_{nm} = H_{nm}/E_0$, $e = E/E_0$, and $E_0 = \hbar^2/2m_0a_0^2 \approx 13.606$ eV, resulting in the following expression for the numerical calculation of the eigenvalues:

$$h_{nm} = \delta\left(\frac{\pi n a_0}{a}\right)^2 - \frac{4\pi^{(1-\frac{\beta}{2})}\Gamma(\beta/2)}{(\beta-2)}\frac{a_0}{a}\Big[G(n+m) - G(n-m)\Big]. \tag{A7}$$

The integrals are computed using trapezoidal integration and the dimensionless Hamiltonian matrix for the FCP model is solved for the first bound states by employing block diagonalization using the Jacobian rule.

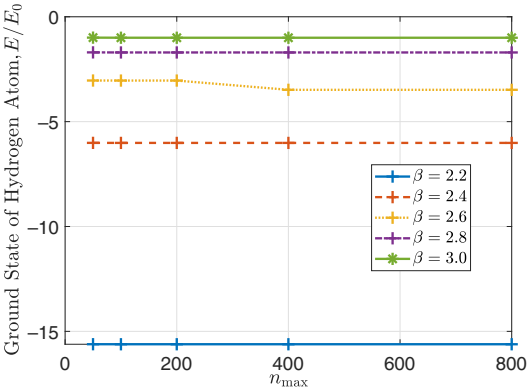

FIG. 11. The FCP-model convergence calculated by varying $n_{\max}$ for $a/a_0 = 20$.

The plots in Figs. 10 and 11 show the convergence of the FCP model for the ground-state energy for $2 < \beta \leq 3$ with respect to a/a_0 and $n_{\max}$, respectively, where $n_{\max}$ represents the Hamiltonian matrix size, which is dependent on the cutoff energy of the wave function, and a/a_0 represents the radial distance equivalent to an infinite QW width, which is important for convergence. We perform our calculation for $n_{\max} = 400$ and $a/a_0 = 50$.

[1] A. Grubiabo, J. A. Miwa, S. S. Grønborg, J. M. Riley, J. C. Johannsen, C. Cacho, O. Alexander, R. T. Chapman, E. Springate, M. Grioni, J. V. Lauritsen, P. D. C. King, P. Hofmann, and S. Ulstrup, Observation of ultrafast free carrier dynamics in single layer MoS_2, Nano Lett. **15**, 5883 (2015).

[2] S. Wu, L. Cheng, and Q. Wang, Excitonic effects and related properties in semiconductor nanostructures: Roles of size and dimensionality, Mater. Res. Express **4**, 085017 (2017).

[3] A. Molina-Sanchez and L. Wirtz, Phonons in single-layer and few-layer MoS_2 and WS_2, Phys. Rev. B **84**, 155413 (2011).

[4] A. Raja, L. Waldecker, J. Zipfel, Y. Cho, S. Brem, J. D. Ziegler, M. Kulig, T. Taniguchi, K. Watanabe, E. Malic, *et al.*, Dielectric disorder in two-dimensional materials, Nat. Nanotechnol. **14**, 832 (2019).

[5] L. Waldecker, A. Raja, M. Rösner, C. Steinke, A. Bostwick, R. J. Koch, C. Jozwiak, T. Taniguchi, K. Watanabe, E. Rotenberg, *et al.*, Rigid Band Shifts in Two-Dimensional Semiconductors through External Dielectric Screening, Phys. Rev. Lett. **123**, 206403 (2019).

[6] M. Pandey, R. Soni, A. Mathur, A. Singh, A. K. Singh, S. Raghavan, and U. Chandni, Noninvasive Subsurface Electrical Probe for Encapsulated Layers in van der Waals Heterostructures, Phys. Rev. Appl. **12**, 064032 (2019).

[7] A. France-Lanord, P. Soukiassian, C. Glattli, and E. Wimmer, Thermal Transport in Supported Graphene: Substrate Effects on Collective Excitations, Phys. Rev. Appl. **7**, 034030 (2017).

[8] D. S. Tanner, J. M. McMahon, and S. Schulz, Interface Roughness, Carrier Localization, and Wave Function Overlap in *c*-Plane (In, Ga) N/Ga N Quantum Wells: Interplay of Well Width, Alloy Microstructure, Structural Inhomogeneities, and Coulomb Effects, Phys. Rev. Appl. **10**, 034027 (2018).

[9] M. I. B. Utama, H. Kleemann, W. Zhao, C. S. Ong, H. Felipe, D. Y. Qiu, H. Cai, H. Li, R. Kou, S. Zhao, *et al.*, A dielectric-defined lateral heterojunction in a monolayer semiconductor, Nat. Electron. **2**, 60 (2019).

[10] V. Carozo, Y. Wang, K. Fujisawa, B. R. Carvalho, A. McCreary, S. Feng, Z. Lin, C. Zhou, N. Perea-López, A. L. Elías, *et al.*, Optical identification of sulfur vacancies: Bound excitons at the edges of monolayer tungsten disulfide, Sci. Adv. **3**, e1602813 (2017).

[11] J. Xiao, M. Zhao, Y. Wang, and X. Zhang, Excitons in atomically thin 2D semiconductors and their applications, Nanophotonics **6**, 1309 (2017).

[12] A. Pospischil and T. Mueller, Optoelectronic devices based on atomically thin transition metal dichalcogenides, Appl. Sci. **6**, 78 (2016).

[13] L. Butov, Excitonic devices, Superlattices Microstruct. **108**, 2 (2017).

[14] C. T. Yip, T. W. Lo, S.-C. Zhu, G. Y. Jia, H. Sun, C.-H. Lam, and D. Lei, Tight-binding modeling of excitonic response in van der Waals stacked 2D semiconductors, Nanoscale Horiz. **4**, 969, (2019).

[15] S. Park, N. Mutz, T. Schultz, S. Blumstengel, A. Han, A. Aljarb, L.-J. Li, E. J. List-Kratochvil, P. Amsalem, and N. Koch, Direct determination of monolayer MoS_2 and WSe_2 exciton binding energies on insulating and metallic substrates, 2D Mater. **5**, 025003 (2018).

[16] A. Steinhoff, J.-H. Kim, F. Jahnke, M. Rösner, D.-S. Kim, C. Lee, G. H. Han, M. S. Jeong, T. O. Wehling, and C. Gies, Efficient excitonic photoluminescence in direct and indirect band gap monolayer MoS_2, Nano Lett. **15**, 6841 (2015).

[17] T. Mueller and E. Malic, Exciton physics and device application of two-dimensional transition metal dichalcogenide semiconductors, NPJ 2D Mater. Appl. **2**, 1 (2018).

[18] K. S. Thygesen, Calculating excitons, plasmons, and quasiparticles in 2D materials and van der Waals heterostructures, 2D Mater. **4**, 022004 (2017).

[19] S. Haastrup, M. Strange, M. Pandey, T. Deilmann, P. S. Schmidt, N. F. Hinsche, M. N. Gjerding, D. Torelli, P. M. Larsen, A. C. Riis-Jensen, *et al.*, The computational 2D materials database: High-throughput modeling and discovery of atomically thin crystals, 2D Mater. **5**, 042002 (2018).

[20] G. Onida, L. Reining, and A. Rubio, Electronic excitations: Density-functional versus many-body Green's-function approaches, Rev. Mod. Phys. **74**, 601 (2002).

[21] D. Y. Qiu, H. Felipe, and S. G. Louie, Optical Spectrum of MoS_2: Many-Body Effects and Diversity of Exciton States, Phys. Rev. Lett. **111**, 216805 (2013).

[22] Y. Lin, X. Ling, L. Yu, S. Huang, A. L. Hsu, Y.-H. Lee, J. Kong, M. S. Dresselhaus, and T. Palacios, Dielectric screening of excitons and trions in single-layer MoS_2, Nano Lett. **14**, 5569 (2014).

[23] J. Frenkel, On the transformation of light into heat in solids. I, Phys. Rev. **37**, 17 (1931).

[24] G. H. Wannier, The structure of electronic excitation levels in insulating crystals, Phys. Rev. **52**, 191 (1937).

[25] T. Olsen, S. Latini, F. Rasmussen, and K. S. Thygesen, Simple Screened Hydrogen Model of Excitons in Two-Dimensional Materials, Phys. Rev. Lett. **116**, 056401 (2016).

[26] Z. Jiang, Z. Liu, Y. Li, and W. Duan, Scaling Universality between Band Gap and Exciton Binding Energy of Two-Dimensional Semiconductors, Phys. Rev. Lett. **118**, 266401 (2017).

[27] X. Yang, S. Guo, F. Chan, K. Wong, and W. Ching, Analytic solution of a two-dimensional hydrogen atom. I. Nonrelativistic theory, Phys. Rev. A **43**, 1186 (1991).

[28] M. Zubair, Y. S. Ang, and L. K. Ang, Thickness dependence of space-charge-limited current in spatially disordered organic semiconductors, IEEE Trans. Electron Devices **65**, 3421 (2018).

[29] M. Zubair, Y. S. Ang, and L. K. Ang, Fractional Fowler-Nordheim law for field emission from rough surface with nonparabolic energy dispersion, IEEE Trans. Electron Devices **65**, 2089 (2018).

[30] M. Zubair and L. Ang, Fractional-dimensional Child-Langmuir law for a rough cathode, Phys. Plasmas **23**, 072118 (2016).

[31] M. Zubair, M. J. Mughal, and Q. A. Naqvi, *Electromagnetic Fields and Waves in Fractional Dimensional Space* (Springer Science & Business Media, New York, 2012).

[32] S. I. Muslih and D. Baleanu, Fractional multipoles in fractional space, Nonlinear Anal. Real World Appl. **8**, 198 (2007).

[33] R. Eid, S. I. Muslih, D. Baleanu, and E. Rabei, On fractional Schrödinger equation in α-dimensional fractional space, Nonlinear Anal. Real World Appl. **10**, 1299 (2009).

[34] F. H. Stillinger, Axiomatic basis for spaces with noninteger dimension, J. Math. Phys. **18**, 1224 (1977).

[35] E. Fortin and F. Raga, Excitons in molybdenum disulphide, Phys. Rev. B **11**, 905 (1975).

[36] A. Laturia, M. L. Van de Put, and W. G. Vandenberghe, Dielectric properties of hexagonal boron nitride and transition metal dichalcogenides: From monolayer to bulk, NPJ 2D Mater. Appl. **2**, 1 (2018).

[37] C. Habenicht, L. Sponza, R. Schuster, M. Knupfer, and B. Büchner, Mapping of the energetically lowest exciton in bulk $1T - HfS_2$, Phys. Rev. B **98**, 155204 (2018).

[38] A. Anedda and E. Fortin, Exciton spectra in $MoSe_2$, J. Phys. Chem. Solids **41**, 865 (1980).

[39] M. M. Ugeda, A. J. Bradley, S.-F. Shi, H. Felipe, Y. Zhang, D. Y. Qiu, W. Ruan, S.-K. Mo, Z. Hussain, Z.-X. Shen, *et al.*, Giant bandgap renormalization and excitonic effects in a monolayer transition metal dichalcogenide semiconductor, Nat. Mater. **13**, 1091 (2014).

[40] X. Cao, B. Clubine, J. Edgar, J. Lin, and H. Jiang, Two-dimensional excitons in three-dimensional hexagonal boron nitride, Appl. Phys. Lett. **103**, 191106 (2013).

[41] A. Arora, M. Drüppel, R. Schmidt, T. Deilmann, R. Schneider, M. R. Molas, P. Marauhn, S. M. de Vasconcellos, M. Potemski, M. Rohlfing, *et al.*, Interlayer excitons in a bulk van der Waals semiconductor, Nat. Commun. **8**, 1 (2017).

[42] A. Beal and W. Liang, Excitons in 2H-WSe_2 and 3R-WS_2, J. Phys. C: Solid State Phys. **9**, 2459 (1976).

[43] A. Beal and H. Hughes, Kramers-Kronig analysis of the reflectivity spectra of 2H-MoS_2, 2H-$MoSe_2$ and 2H-$MoTe_2$, J. Phys. C: Solid State Phys. **12**, 881 (1979).

[44] L. Museur, G. Brasse, A. Pierret, S. Maine, B. Attal-Trétout, F. Ducastelle, A. Loiseau, J. Barjon, K. Watanabe, T. Taniguchi, *et al.*, Exciton and interband optical transitions in hBN single crystal, arXiv:1102.5017 (2011).

[45] W. Shan, B. Little, A. Fischer, J. Song, B. Goldenberg, W. Perry, M. Bremser, and R. Davis, Binding energy for the intrinsic excitons in wurtzite GaN, Phys. Rev. B **54**, 16369 (1996).

[46] H. Asahina and A. Morita, Band structure and optical properties of black phosphorus, J. Phys. C: Solid State Phys. **17**, 1839 (1984).

[47] T. Cheiwchanchamnangij and W. R. Lambrecht, Quasiparticle band structure calculation of monolayer, bilayer, and bulk MoS_2, Phys. Rev. B **85**, 205302 (2012).

[48] See the Supplemental Material at http://link.aps.org/supplemental/10.1103/PhysRevApplied.13.064062 for [details of binding-energy calculations for a comparative analysis of the proposed FCP model].
[49] M. Trushin, Tightly bound excitons in two-dimensional semiconductors with a flat valence band, Phys. Rev. B **99**, 205307 (2019).
[50] I. Pelant and J. Valenta, *Luminescence Spectroscopy of Semiconductors* (Oxford University Press, New York, 2012).
[51] G. Y. Jia, Y. Liu, J. Y. Gong, D. Y. Lei, D. L. Wang, and Z. X. Huang, Excitonic quantum confinement modified optical conductivity of monolayer and few-layered MoS_2, J. Mater. Chem. C **4**, 8822 (2016).
[52] X. Li and H. Zhu, Two-dimensional MoS_2: Properties, preparation, and applications, J. Materiomics **1**, 33 (2015).
[53] T. C. Berkelbach, M. S. Hybertsen, and D. R. Reichman, Theory of neutral and charged excitons in monolayer transition metal dichalcogenides, Phys. Rev. B **88**, 045318 (2013).
[54] R.-Z. Li, X.-Y. Dong, Z.-Q. Li, and Z.-W. Wang, Correction of the exciton Bohr radius in monolayer transition metal dichalcogenides, Solid State Commun. **275**, 53 (2018).
[55] G. Berghäuser and E. Malic, Analytical approach to excitonic properties of MoS_2, Physical. Rev. B **89**, 125309 (2014).
[56] H.-W. Li, Z. Guan, Y. Cheng, T. Lui, Q. Yang, C.-S. Lee, S. Chen, and S.-W. Tsang, On the study of exciton binding energy with direct charge generation in photovoltaic polymers, Adv. Electron. Mater. **2**, 1600200 (2016).
[57] X. Liu, Y. Li, K. Ding, and S. Forrest, Energy Loss in Organic Photovoltaics: Nonfullerene versus Fullerene Acceptors, Phys. Rev. Appl. **11**, 024060 (2019).
[58] A. Thilagam, Exciton complexes in low dimensional transition metal dichalcogenides, J. Appl. Phys. **116**, 053523 (2014).
[59] A. Kumar and P. Ahluwalia, Tunable dielectric response of transition metals dichalcogenides MX_2 (M = Mo, W; X = S, Se, Te): Effect of quantum confinement, Physica B Condens. Matter **407**, 4627 (2012).
[60] P. Zhao, H. Yang, J. Li, H. Jin, W. Wei, L. Yu, B. Huang, and Y. Dai, Design of new photovoltaic systems based on two-dimensional group-IV monochalcogenides for high performance solar cells, J. Mater. Chem. A **5**, 24145 (2017).
[61] M. Massicotte, F. Vialla, P. Schmidt, M. B. Lundeberg, S. Latini, S. Haastrup, M. Danovich, D. Davydovskaya, K. Watanabe, T. Taniguchi, *et al.*, Dissociation of two-dimensional excitons in monolayer WSe 2, Nat. Commun. **9**, 1 (2018).
[62] A. Pospischil, M. M. Furchi, and T. Mueller, Solar-energy conversion and light emission in an atomic monolayer *p-n* diode, Nat. Nanotechnol. **9**, 257 (2014).
[63] B. Godefroid and G. Kozyreff, Design of Organic Solar Cells as a Function of Radiative Quantum Efficiency, Phys. Rev. Appl. **8**, 034024 (2017).
[64] Y.-W. Zhang, J.-Y. Li, C.-H. Wu, C.-Y. Chang, S.-W. Chang, M.-H. Shih, and S.-Y. Lin, Tungsten diselenide top-gate transistors with multilayer antimonene electrodes: Gate stacks and epitaxially grown 2D material heterostructures, Sci. Rep. **10**, 1 (2020).
[65] Z. Qiu, M. Trushin, H. Fang, I. Verzhbitskiy, S. Gao, E. Laksono, M. Yang, P. Lyu, J. Li, J. Su, *et al.*, Giant gate-tunable bandgap renormalization and excitonic effects in a 2D semiconductor, Sci. Adv. **5**, eaaw2347 (2019).
[66] A. Raja, A. Chaves, J. Yu, G. Arefe, H. M. Hill, A. F. Rigosi, T. C. Berkelbach, P. Nagler, C. Schüller, T. Korn, *et al.*, Coulomb engineering of the bandgap and excitons in two-dimensional materials, Nat. Commun. **8**, 1 (2017).
[67] W.-h. Guo, J.-j. Shi, Y.-h. Zhu, M. Wu, J. Du, Y.-l. Cen, S.-m. Liu, and S.-p. Han, Two-Dimensional 111-Type In-Based Halide Perovskite Cs_3 In_2 X_9(X= Cl, Br, I) with Optimal Band Gap for Photovoltaics and Defect-Insensitive Blue Emission, Phys. Rev. Appl. **13**, 024031 (2020).
[68] G. Zhang, A. Chaves, S. Huang, F. Wang, Q. Xing, T. Low, and H. Yan, Determination of layer-dependent exciton binding energies in few-layer black phosphorus, Sci. Adv. **4**, eaap9977 (2018).
[69] H. Shi, H. Pan, Y.-W. Zhang, and B. I. Yakobson, Quasiparticle band structures and optical properties of strained monolayer MoS_2 and WS_2, Phys. Rev. B **87**, 155304 (2013).
[70] H. Moon, G. Grosso, C. Chakraborty, C. Peng, T. Taniguchi, K. Watanabe, and D. Englund, Dynamic exciton funneling by local strain control in a monolayer semiconductor, arXiv:1906.10077 (2019).
[71] O. B. Aslan, I. M. Datye, M. J. Mleczko, K. Sze Cheung, S. Krylyuk, A. Bruma, I. Kalish, A. V. Davydov, E. Pop, and T. F. Heinz, Probing the optical properties and strain-tuning of ultrathin $Mo_{1-x}W_xTe_2$, Nano Lett. **18**, 2485 (2018).
[72] M. Feierabend, A. Morlet, G. Berghäuser, and E. Malic, Impact of strain on the optical fingerprint of monolayer transition-metal dichalcogenides, Phys. Rev. B **96**, 045425 (2017).
[73] W. Song and L. Yang, Quasiparticle band gaps and optical spectra of strained monolayer transition-metal dichalcogenides, Phys. Rev. B **96**, 235441 (2017).
[74] B. Jugdutt and F. Marsiglio, Solving for three-dimensional central potentials using numerical matrix methods, Am. J. Phys. **81**, 343 (2013).